Urban Climate 18 (2016) 58–72

Contents lists available at ScienceDirect

Urban Climate

journal homepage: http://www.elsevier.com/locate/uclim

Microscale mobile monitoring of urban air temperature

Pak Keung Tsin, MSc [a,*], Anders Knudby, PhD [b], E. Scott Krayenhoff, PhD [c], Hung Chak Ho, PhD [d], Michael Brauer, ScD [a], Sarah B. Henderson, PhD [a,e]

[a] School of Population and Public Health, University of British Columbia, Vancouver, BC, Canada
[b] Department of Geography, Environment and Geomatics, University of Ottawa, Ottawa, ON, Canada
[c] Department of Geography, Western University, London, ON, Canada
[d] Department of Geography, Simon Fraser University, Burnaby, BC, Canada
[e] BC Centre for Disease Control, Vancouver, BC, Canada

ARTICLE INFO

Article history:
Received 6 April 2016
Received in revised form 1 October 2016
Accepted 12 October 2016

Keywords:
Hot weather
Air temperature
Mobile monitoring
Spatial variability
Microscale measurements

ABSTRACT

Background: Mobile air temperature monitoring is a promising method to better understand temperature distributions at fine spatial resolutions across urban areas. The study objectives were to collect microscale measurements for evaluate different data sources used to assess heat exposure in greater Vancouver, Canada.

Methods: Mobile air temperature monitoring was conducted on foot at least twice for each of 20 routes. First, the mobile data were compared with 1-minute measurements from the nearest fixed site. Second, the mobile data from runs corresponding with Landsat overpass days were compared with satellite-derived land surface temperature (LST). Third, the mobile data were compared with estimates from a previously developed heat map for the region.

Results: Mobile measurements were typically higher and more variable than simultaneous fixed site measurements. Correlations between mobile measurements and LST were weak and highly variable (r^2 = 0.04–0.38). The z-score differentials between mobile measurements and the heat map suggested that spatial variability in temperatures is captured by the heat map.

Conclusion: Microscale measurements confirm that fixed sites do not characterize the variability in thermal conditions within nearby streetscapes. Microscale monitoring of air temperatures is a valuable tool for

* Corresponding author at: 10095 Lawson Dr, Richmond V7E 5M2, BC, Canada.
E-mail address: roberttsin@alumni.ubc.ca (P.K. Tsin)

http://dx.doi.org/10.1016/j.uclim.2016.10.001

temporally and spatially evaluating other high resolution temperature data within small areas.

1. Introduction

Extreme hot weather events have been associated with significant excess morbidity and mortality worldwide, especially in urban areas (Zhang et al., 2014; Harlan et al., 2006; Kalkstein and Davis, 1989; Robine et al., 2008; Luber and McGeehin, 2008; Lugo-Amador et al., 2004; Intergovernmental Panel on Climate Change, 2014). These events are typically defined as consecutive days with maximum and minimum air temperatures above the normal climatic range, which varies by location (Harlan et al., 2006; Meehl and Tebaldi, 2004). Some important and well-documented examples include >700 deaths during the 1995 heatwave in Chicago (Semenza et al., 1996; Kaiser et al., 2007), >30,000 deaths during the 2003 heatwave in Europe (Robine et al., 2008; García-Herrera et al., 2010; Sardon, 2007), and >15,000 deaths during the 2010 heatwave in Russia (Barriopedro et al., 2011; Shaposhnikov et al., 2014). During the summer of 2009 a much smaller event in greater Vancouver, Canada, was associated with an estimated 110 excess deaths, which corresponded to a 40% increase in mortality when compared with previous summer weeks (Henderson and Kosatsky, 2012; Kosatsky et al., 2012).

Most epidemiologic analyses of such events use fixed site air temperature measurements from stations maintained by local, regional, or federal government agencies responsible for the environment (Robine et al., 2008; Kaiser et al., 2007; García-Herrera et al., 2010; Barriopedro et al., 2011; Shaposhnikov et al., 2014; Henderson and Kosatsky, 2012; Kosatsky et al., 2012). While the quality of these data is high, the ability of these data to reflect the temperature variability experienced by urban populations is generally low because they are measured at the local scale (100–3000 m) or mesoscale (3000–100,000 m) (Oke, 2004; Oke, 1987; World Meteorological Organization, 2008). In addition, these stations are often located in open areas to ensure no interference from shading (World Meteorological Organization, 2008), so they do not reflect the distribution of populations, nor of built environments that can generate urban heat island (UHI) effects. In reality, air temperature varies at the microscale (<100 m) and the local scale (100–3000 m) (Saaroni and Ziv, 2010; Nichol and To, 2012), and the health risks associated with extremely hot weather are assumed to vary with the exposure.

To overcome the limitations of fixed site measurements, some studies have attempted to model spatial variability in urban air temperatures using remote sensing data or spatial models that integrate data from multiple sources. Many of these studies have used remote sensing measurements of land surface temperature (LST) from platforms such as the Moderate Resolution Imaging Spectroradiometer (MODIS) and Landsat (Sohrabinia et al., 2014; Gallo et al., 2010; Benali et al., 2012). Some have used mobile monitoring by vehicle or bicycle (Saaroni and Ziv, 2010; Cassano, 2013; Oke and Maxwell, 1967). Others have focused on the relationships between air temperature and geographic variables such as distance from the coast, sky-view factor, and surface cover (Eliasson and Svensson, 2003; Rinner and Hussain, 2011). For example, the greater Vancouver heat map (GVHM) used variables such as Landsat LST and sky-view factor to estimate the spatial variability in regional air temperatures on very hot days at a resolution of 60 m (Ho et al., 2016a). The map was developed primarily for spatial delineation of health risks within the region, and has been evaluated for that purpose (Ho et al., 2016b).

Spatial temperature models such as the GVHM are typically built using data from fixed monitoring sites as both the dependent variable and the validation data, with remote sensing measurements such as LST as one or more of the independent variables (Ho et al., 2016a; Nichol et al., 2009; Nichol and Wong, 2008). Because the spatial resolution of the satellite data is often at the microscale (<100 m), the maps themselves display spatial variability within the same scale but are rarely evaluated with microscale measurements. Furthermore, there is little information on how well the combination of fixed site and remote sensing inputs actually captures the microscale variability that the resulting maps purport to reflect. The general objective of our study was to address these uncertainties through the collection and analysis of microscale air temperature data, and comparison of those data to the independent and dependent variables frequently used in high resolution temperature mapping, as well as the estimates from such a model. More specifically, temperature data from 20 routes in

greater Vancouver were compared with: (1) fixed site measurements at the nearest locations; (2) Landsat LST measurements taken on the same day, where available; and (3) estimates from the GVHM.

2. Methods

2.1. Study area and population

The greater Vancouver urban area is located on the southwest coast of the Canadian province of British Columbia, in the Fraser River delta. The 2011 population was 2.3 million residents, with an average year-over-year increase of 1.9% (Statistics Canada, 2012). Typical summer weather is characterized by low pressure, anti-cyclonic systems that are associated with warm, sunny conditions and light winds (Oke and Hay, 1994). However, there are occasional rainy summer periods when a cyclonic system affects the area (Oke and Hay, 1994). Because greater Vancouver is bounded by mountain ridges in the north, the Pacific Ocean in the west, and the Fraser Valley in the east, complementary mesoscale land-sea breeze and mountain-valley circulation systems are commonly present in summer (Oke and Hay, 1994; Richards, 2005).

2.2. Route selection

We selected 20 walking routes with an approximate length of 8–10 km per route, which would allow each to be walked in 2–3 h (Fig. 1). Route selection was based on factors that could increase individual vulnerability to heat stress. Specifically, walking routes were chosen in areas that fulfilled either of the following criteria: (1) two of the listed conditions below were met for at least 30% of the area, or (2) one of the listed conditions below was met for at least 75% of the area. The conditions were: (1) a population density > 100 persons/ha as determined from the 2006 census (Statistics Canada, 2008; Sauder, 2010); (2) an estimated air temperature >3.5 °C warmer than Vancouver International Airport (YVR) according to the GVHM (Ho et al., 2016a); and (3) an average household income below $30,000 from the 2006 census (Statistics Canada, 2008; Sauder, 2010). Census tracts with zero income occurred when census results had been suppressed, so population density and GVHM were used as the only selection criteria in these areas. After initial identification, the final walking routes were spatially distributed across the study area to maximize coverage, especially in areas with sparse fixed monitoring data. The routes were also selected to provide a range of distances to the nearest major bodies of water. Routes were created manually by retaining streets that optimized logistical efficiency (Fig. 1). In addition to providing the Local Climate Zone (LCZ) categories (Mills and Foley, 2016) for each route and weather station (Table 1), we have also provided a keyhole markup language (KML) file (Fig. S.1 in Supplementary material).

2.3. Mobile air temperature data collection

Mobile temperature data were collected on foot using a Met One 064-2 temperature sensor inside a radiation shield, a Kestrel 4500 Portable Weather Station, a GoPro Hero 3 video camera, and a Garmin GPSMAP 78s GPS (Fig. 2). The Met One 064-2 and Kestrel 4500 were mounted to a PVC pipe frame at a height of 1.5 m and a distance of 50 cm away from the body to prevent direct heat transfer. The Kestrel and GoPro video data were not used in the analyses presented here. The Met One 064-2 temperature sensor was chosen for this study because its technical specifications indicate an accuracy of ± 0.1 °C and a response time of 10 s in still air (Met One Instruments, Inc. MODEL 064-1, 064-2, 2005). Our walking speed calculations and our Kestrel 4500 data indicate that there was approximately 1.2 m/s of ventilation for the air temperature sensor. Our preliminary testing indicated that, at walking speed, the sensor responded to a 2 °C fluctuation within 10 s and returned to 70% of baseline within 30 s, returning to baseline required 5 min (unpublished data). All data were logged at 10 second intervals. Study data were collected on foot for two reasons. First, travelling by foot means smaller distances were covered within set time periods compared with travelling by vehicle or bike, which allows higher spatial resolution. Second, many areas were only accessible by pedestrians or bicycles in greater Vancouver due to transportation network design.

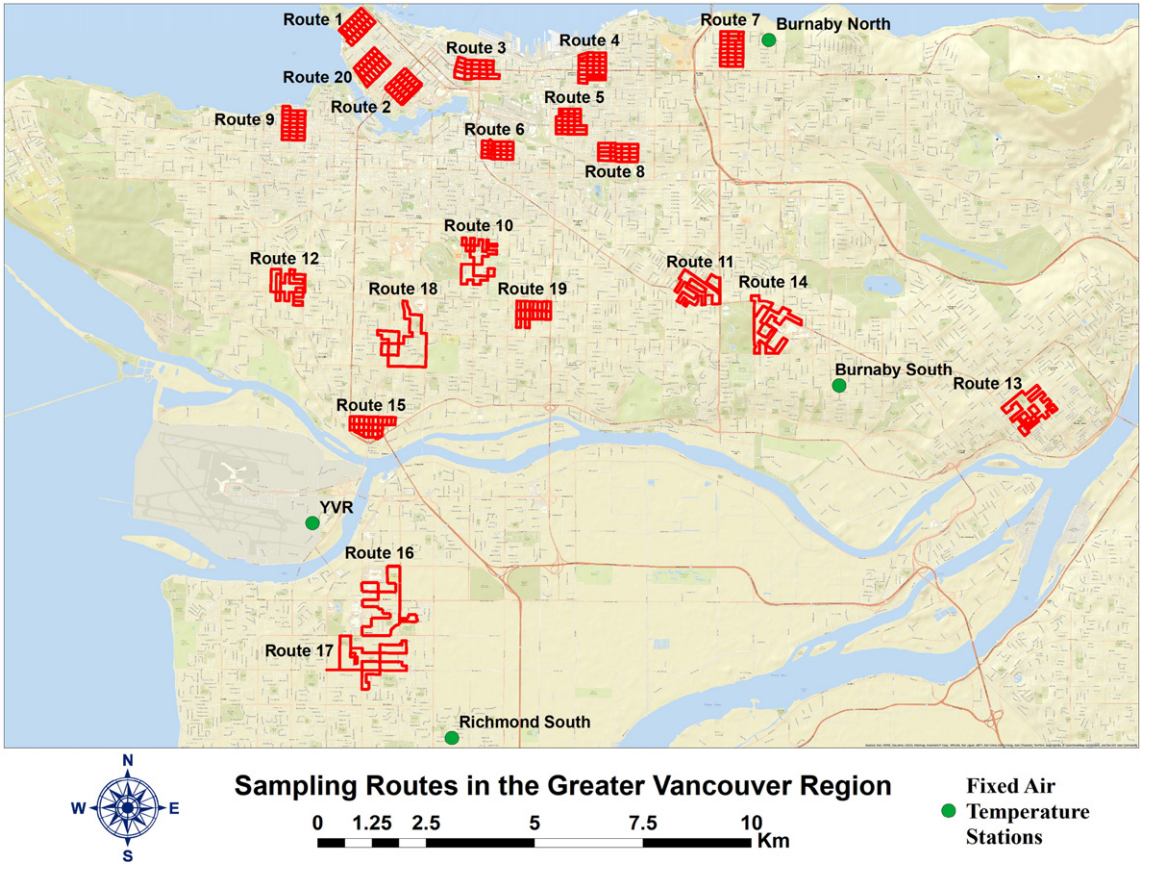

Fig. 1. Map of all 20 greater Vancouver mobile air temperature sampling routes and all Metro Vancouver fixed stations used in this study. The Burnaby North and Richmond South stations were in grass fields located in residential neighbourhoods with detached dwellings. The Burnaby South station was on a school rooftop in a residential neighbourhood with detached dwellings, and the Vancouver International Airport (YVR) station was in a grass field hundreds of meters from an airport runway (Metro Vancouver, 2012).

Table 1
Station air temperature sensor heights and Local Climate Zone classifications for each site (Mills and Foley, 2016; Metro Vancouver, 2012).

Site name	Air temperature sensor height (m)	Local climate zone
Fixed sites		
Richmond South	8.2	9-sparsely built
Burnaby South	19.3	8-large low-rise
Burnaby North	5.7	4-open high-rise
YVR	5.5	E-bare rock or paved
Mobile routes		
Route 1	1.5	5-open mid-rise
Route 2	1.5	2-compact mid-rise
Route 3	1.5	3-compact low-rise
Route 4	1.5	4-open high-rise
Route 5	1.5	6-open low-rise
Route 6	1.5	6-open low-rise
Route 7	1.5	4-open high-rise
Route 8	1.5	6-open low-rise
Route 9	1.5	4-open high-rise
Route 10	1.5	6-open low-rise
Route 11	1.5	4-open high-rise
Route 12	1.5	4-open high-rise
Route 13	1.5	5-open mid-rise
Route 14	1.5	4-open high-rise
Route 15	1.5	5-open mid-rise
Route 16	1.5	4-open high-rise
Route 17	1.5	6-open low-rise
Route 18	1.5	6-open low-rise
Route 19	1.5	6-open low-rise
Route 20	1.5	5-open mid-rise

We collected 42 sets of data for the 20 sampling routes, with each route monitored at least twice. All data collection was conducted from May to September 2014, between the hours of 15:00 and 18:00 to capture the hottest hours of summer days in the region. Data collection occurred mainly on days when the maximum air temperature exceeded 22 °C at YVR to ensure high temperatures were present in the dataset. Overcast days

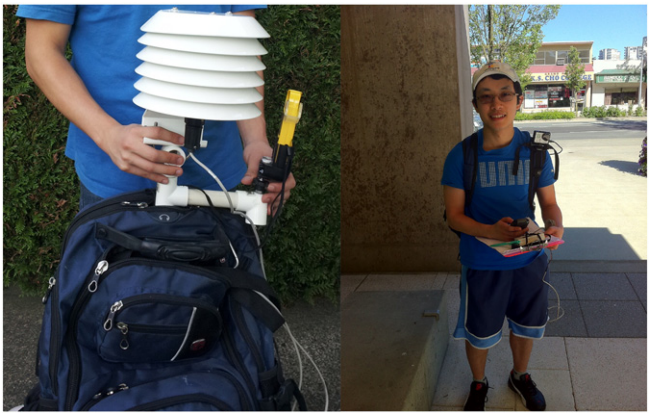

Fig. 2. Mobile monitoring setup. Left image shows the white radiation shield containing the Met One 064-2 sensor and the yellow Kestrel 4500 Portable Weather Station. The right image shows the typical sampling setup with the thermometers worn and the GoPro video camera mounted on the left shoulder.

were not sampled, and any periods of cloudiness that occurred during a sampling run were manually recorded. Instrument times were synchronized prior to each run to maximize temporal matching. Replicate runs of each route were designed such that they were walked on the opposite side of the street and in opposite directions from each other.

2.4. Temperature data for comparison with microscale measurements

We compared mobile measurements with three different sources of temperature data: (1) fixed site air temperature measurements from the local monitoring network; (2) Landsat measurements of LST; and (3) hot day air temperature estimates from the GVHM. Fixed air temperature measurements at 1-minute intervals were received for four sites (Fig. 1 and Fig. S.1 in Supplementary material) from Metro Vancouver, which is a partnership providing joint services to all the municipalities in the region (Metro Vancouver, 2015). The fixed site air temperature sensors had heights ranging from 5.5 m at YVR to 19.3 m at Burnaby South, and all instruments were within the urban canopy layer for their respective areas (Table 1) (Metro Vancouver, 2012).

Landsat satellite images are publicly available and can be processed into multiple products, including LST (USGS, 2012; NASA, 2014). Level 1 data from June 3 (Landsat 7), July 13 (Landsat 8), and July 29 (Landsat 8) 2014, all acquired at approximately 11:00 pacific standard time, were obtained from the US Geological Service (U.S. Geological Survey, 2015a). These data were collected 4–7 h prior to the spatially matched mobile data, which were measured during the hottest hours of the day. We chose to conduct the comparison this way because it was consistent with the use of LST data in the GVHM, which also modelled air temperature during the hottest hours of a typical hot summer day. While Landsat thermal data are originally sampled at horizontal resolutions of 60 m (Landsat 7) or 100 m (Landsat 8) at nadir, they are resampled and provided to users at a 30-meter spatial resolution, which was used for our analyses (USGS, 2016a). All three images were processed into LST values using established methods (Ho et al., 2016a; Irons and Taylor, 2011; U.S. Geological Survey, 2013) in the R statistical computing environment (R Core Team, 2014). These methods included a correction for thermal emissivity using normalized differential vegetation index (NDVI) values (Van de Griend and Owe, 1993), and a conversion from top of atmosphere temperature values to LST values (Barsi et al., 2003; Markham and Barsi, 2014). The Landsat 7 data gaps due to the scan line corrector error were left as is (U.S. Geological Survey, 2015b), while the Landsat 8 stray light effect was minimized by using band 10 as the thermal band (USGS, 2016b).

The GVHM (Ho et al., 2016a) was constructed using a random forest algorithm, which modelled the relationship between maximum air temperature at 59 weather stations and several predictor variables. Random forest is a non-parametric machine learning method which uses a large number of regression trees to model such relationships (Ho et al., 2016a; Gislason et al., 2006). The predictor variables in the GVHM we used were LST averaged within a 1000 m buffer, distance from the ocean, elevation, normalized difference water index, sky-view factor, solar radiation, and water vapor (Ho et al., 2016a). The Landsat LST data used in the GVHM were restricted to six hot days with air temperatures exceeding 25 °C at the YVR fixed site (Ho et al., 2016a). This restriction was made because the GVHM was designed to reflect spatial variation in air temperature on relatively hot days in the region. The map performed well at the local and mesoscale when compared with similar products for other cities (Ho et al., 2016a). The published map expresses modelled temperatures relative to YVR because it is the station most frequently reported by the media, but we used the map of absolute values for this study.

2.5. Data analysis

All data analysis and mapping were conducted with R version 3.1.0 and ESRI ArcGIS 10.2 (R Core Team, 2014; Esri, 2014). To compare the mobile air temperatures with the nearest fixed site air temperatures we generated 1-minute time series plots for each run and calculated the following variables: mean and standard deviation (SD) mobile temperature; mean and SD fixed temperature; mean and SD difference between each 10-second value and the closest 1-minute value.

Because mobile temperatures were measured over the course of 2–3 h during the hottest period of the day, there was typically an increase in ambient temperature over the measurement period. Given our interest in the spatial rather than temporal variability for comparison with the LST and GVHM data, we adjusted for

these short-term temporal trends (Eq. (1)). The reference site used was the Metro Vancouver fixed weather station data at YVR (Fig. 1) (Metro Vancouver, 2014).

$$T_{run\ adj} = \frac{T_{sampling,raw}}{T_{ref\ site,rolling} \Big/ T_{ref\ site,run\ mean}} \quad (1)$$

where: $T_{run\ adj}$ is the adjusted mobile air temperature in 10-second intervals; $T_{sampling,\ raw}$ is the raw mobile sampling air temperature in 10-second intervals; $T_{refsite,\ rolling}$ is the reference site air temperature centered rolling mean (over 1 min intervals), time matched with $T_{sampling,\ raw}$; $T_{ref\ site,\ run\ mean}$ is the overall mean for the reference site air temperature during the same period when $T_{sampling,\ raw}$ was collected.

After the mobile air temperature data were adjusted, they were rasterized to a 30-meter resolution by taking the average of all point values within each cell. To compare the rasterized mobile data with the rasterized LST data, we generated scatter plots of the spatially matched values for the three sampling dates covered by Landsat, and histograms showing the LST distributions on each day were also generated. The coefficient of determination (r^2), its *p*-value, the line of best fit, and the LST/mobile air temperature difference were calculated for each plot. The r^2 indicates how much of the variation in air temperature is explained by the variation in LST, while the *p*-value indicates the likelihood of the relationship being observed by chance alone.

The mobile data were collected on 42 summer days, whereas the GVHM was developed to reflect a typical hot summer day in greater Vancouver (Ho et al., 2016a). To compare the rasterized mobile data with the rasterized GVHM data we converted both to z-scores, which indicate how many standard deviations each value is from the mean of its distribution. The use of z-scores allowed us to compare relative air temperatures between the mobile and GVHM datasets. Each individual mobile air temperature value was converted to z-score based on the mean and standard deviations for its specific run. Each individual GVHM value was converted to a z-score by cropping the entire GVHM raster to the extent of each route, and using the mean and standard deviation of the cropped area. The difference between the GVHM z-scores and the mobile z-scores was calculated to create z-score differential maps for each run. Finally, correlation values for each run were calculated by taking spatially-matched mobile air temperature z-score data from two replicates of each run, creating a scatterplot for that run, and then calculating the correlation,

3. Results

3.1. Mobile data compared with fixed site data

Complete 10-second interval air temperature datasets were collected for 41 out of 42 runs, while run 4B had data that was collected at 1 minute intervals due to an instrument error. The routes ranged in length from 6.4 km (route 6) to 9.9 km (route 17), and in area from 0.5 km^2 (route 6) to 2.5 km^2 (route 16) (Table S.1, Supplementary material). As expected, mobile air temperature measurements were typically higher and more variable than simultaneous air temperature measurements at the nearest fixed site (Fig. 3, Table S.1). There was little consistency between replicate measurements on the same route, possibly due to differences in meteorology and regional thermal state on the different measurement days, and possibly due to the fact that replicates were measured in opposite directions and on opposite sides of the street. The fixed stations did generally characterize short-term temporal trends of nearby routes, even when the closest station was almost 10 km away (Fig. 1). The trends were most similar when the distance between the fixed site and the route was short. However, even for routes that were <1 km from the nearest fixed site (7A and B), there was considerable variability in the mobile measurements that was not evident in the fixed station measurements.

3.2. Mobile data compared with land surface temperature data

Landsat satellites overpassed the study area on June 3, July 13, and July 29, which corresponded with runs 15A, 18B, and 12B, respectively. Run 15A was monitored between 4:19–6:39 PM, run 18B was monitored between 4:01–5:53 PM, and run 12B was monitored between 3:36–5:22 PM. The mean temperatures at YVR

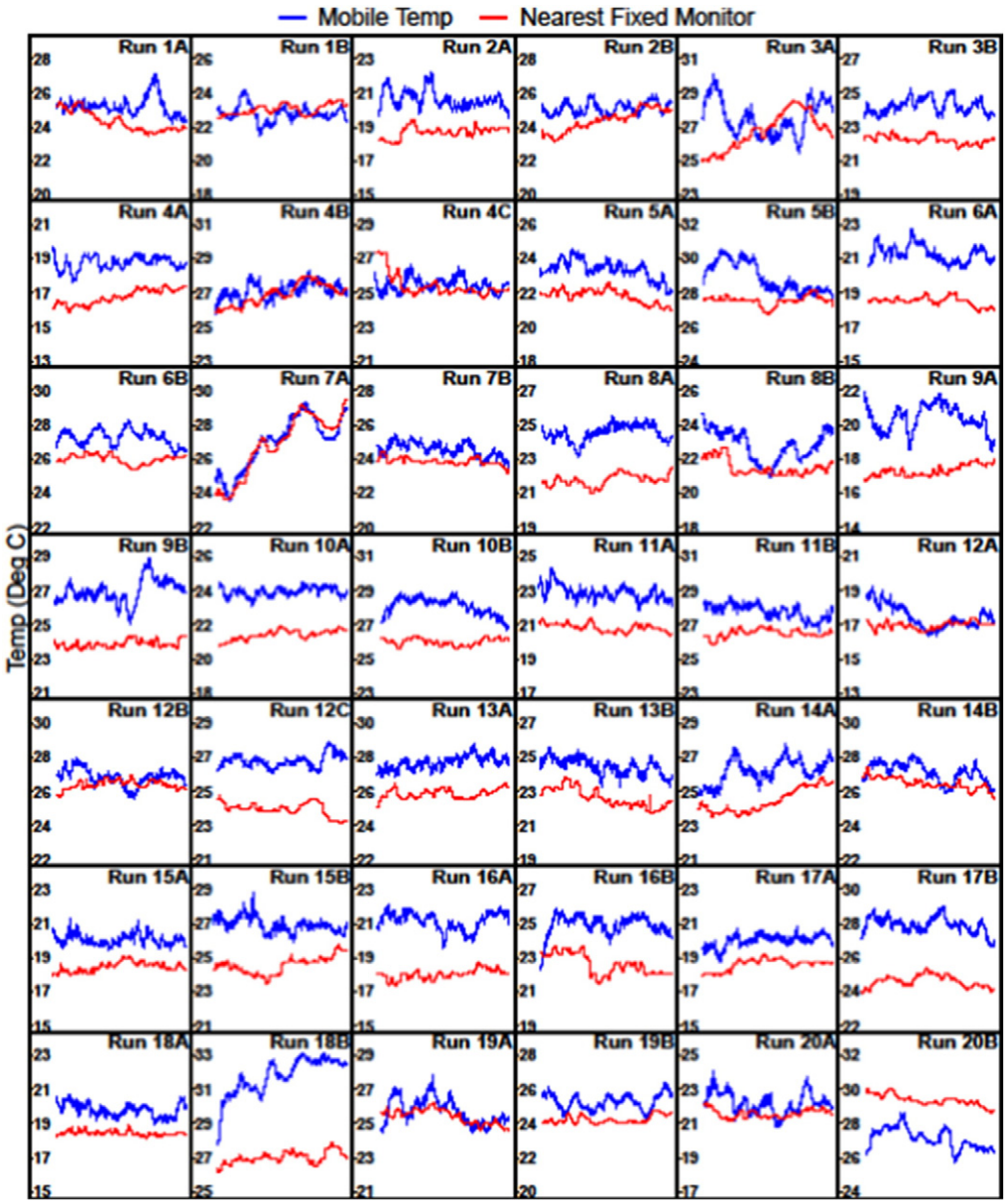

Fig. 3. Raw mobile air temperature (red) from mobile runs and air temperature from the closest Metro Vancouver weather station (blue). Y-axis shows temperature in °C while the x-axis shows time (see Table S.1 in Supplementary material for run durations). Note that both x-axis and y-axis scales vary from run to run.

during those runs were 18.5 °C, 27.0 °C, and 26.4 °C, and the mean mobile air temperatures for those runs were 20.1 °C, 31.9 °C, and 26.8 °C respectively. In comparison, the mean LST values were 35.1 °C for run 15A, 38.1 °C for run 18B, and 34.8 °C for run 12B. Runs 15A and 12B were both sunny throughout, while route 18B was sunny with intermittent cloudiness. The linear regression relationship between the mobile

air temperatures and LSTs were weak (Fig. 4), and there was no clear similarity between the three runs. The relationship with LST was likely driven by route location, as the correlations on the matched overpass days were similar to those on the unmatched days, with the exception of route 12B (Table 2).

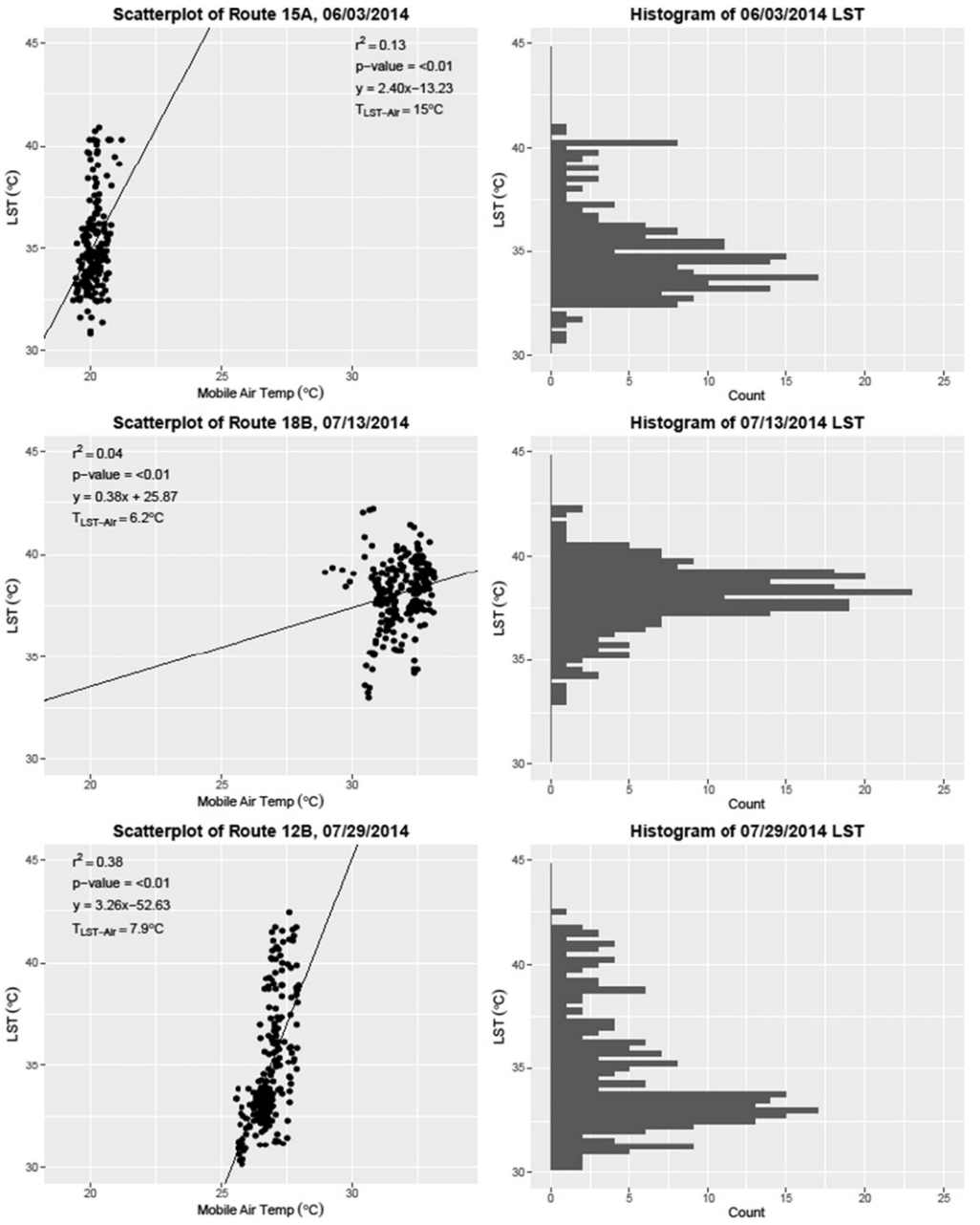

Fig. 4. Scatter plot of mobile air temperature and LST as well as the LST histogram for mobile monitoring runs coinciding with Landsat overpass days. The r^2 value between mobile air temperature and LST, the *p*-value for the calculated r^2 value, the fit line equation, and the mean temperature difference between LST and mobile air temperature are provided on each plot. The LST data were measured at approximately 11:00, while the mobile air temperature data were mostly measured between 15:00 and 18:00.

Table 2
Correlation values between mobile run air temperature data and LST from all three overpass dates. Bold values indicate the correlation on the matched date.

	LST from three overpass dates		
Mobile run	June 3 (Run 15A)	July 13 (Run 18B)	July 29 (Run 12B)
15A	**0.37**	0.31	0.27
18B	0.22	**0.20**	0.16
12B	0.00	0.64	**0.61**

3.3. Mobile data compared with the greater Vancouver heat map (GVHM)

When the z-scores of mobile measurements were compared with the z-scores of the GVHM estimates, the correlation between run replicates varied from route to route, but most run replicates were similar in visual comparison (Fig. 5). The mean correlation (r) between route replicates z-scores was 0.46, the maximum correlation was 0.83, and the minimum correlation was −0.01 (see Fig. S.2 in Supplementary material for correlations and scatterplots of all runs). The GVHM described spatial variability in air temperatures for parts of many routes, as indicated by the large areas that were in agreement (Fig. 5).

The total number of raster cells between all 42 runs was 11,379. Of these, 57.4% had a z-score between −1 and 1, 23.3% had a z-score > 1, and 19.3% had a z-score < −1 (Table S.2, Supplementary material). Route 16A had the largest percentage of cells with z-scores > 1 (32.3%, 41.9% between −1 and 1, and 25.8% < −1). Route 18B had the largest percentage of cells with z-scores between −1 to 1 (76.5%, 17.9% > 1, and 5.6% < −1). Route 8A had the largest percentage of cells with z-scores < −1 (32.9%, 39.2% between −1 and 1, and 27.9% > 1). Of the 42 runs, 33 had over 50% of raster cells with z-scores between −1 and 1 (Table S.2), which suggests the GVHM generally captured the spatial variability in air temperatures.

4. Discussion

There is limited evidence on the relationships between microscale urban air temperature measurements and other existing methods for measuring or modelling air temperature. Comparisons between mobile and fixed site air temperatures indicated that mobile measurements were generally higher than time-synchronized fixed site measurements. Comparison between mobile air temperatures and LST showed that the two variables were positively correlated, although the relationships were weak. Finally, comparison between mobile air temperatures and the GVHM suggested that the GVHM captured spatial variability in temperatures on many routes, but that it underestimated and overestimated variation in some areas when compared with measured data.

Some previous studies have measured both fixed and mobile air temperatures (Straka et al., 1996; Hedquist and Brazel, 2006), but we found none that had compared these two variables directly. Although the differences we observed were expected, we report them here to provide others with some information about the range of variability that might be found in other contexts. The differences are likely driven by the built environment (Saaroni and Ziv, 2010; Oke and Maxwell, 1967; Emmanuel and Krüger, 2012; Holmer et al., 2007; Oke, 1982; Watkins et al., 2007), because most mobile monitoring routes were in urban areas, while the fixed weather stations were in less developed areas. In addition, temperatures at the fixed stations were potentially cooler due to vertical temperature gradients. The mobile air sensor was mounted at a height of 1.5 m, while the fixed station temperature sensors were at heights of 5.5–19.3 m (Table 1). The differences between fixed site and mobile measurements highlight the reality that heat-related health risks are likely to vary with the exposure, and that the limitations of fixed site data should be acknowledged when considering public health. Many epidemiologic studies use these data to reflect population exposures (Robine et al., 2008; Kaiser et al., 2007; García-Herrera et al., 2010; Barriopedro et al., 2011; Shaposhnikov et al., 2014; Henderson and Kosatsky, 2012; Kosatsky et al., 2012), but estimates that are more representative at the microscale, such as heat maps, may result in better models and more targeted interventions (Ho et al., 2016b).

The r^2 values we report for the relationship between mobile air temperature and LST (0.04–0.38) were lower than those reported in previous studies. These ranged from 0.64–0.87 when LST was compared with time-matched air temperature (Sohrabinia et al., 2014; Gallo et al., 2010; Nichol et al., 2009) or 0.83 when

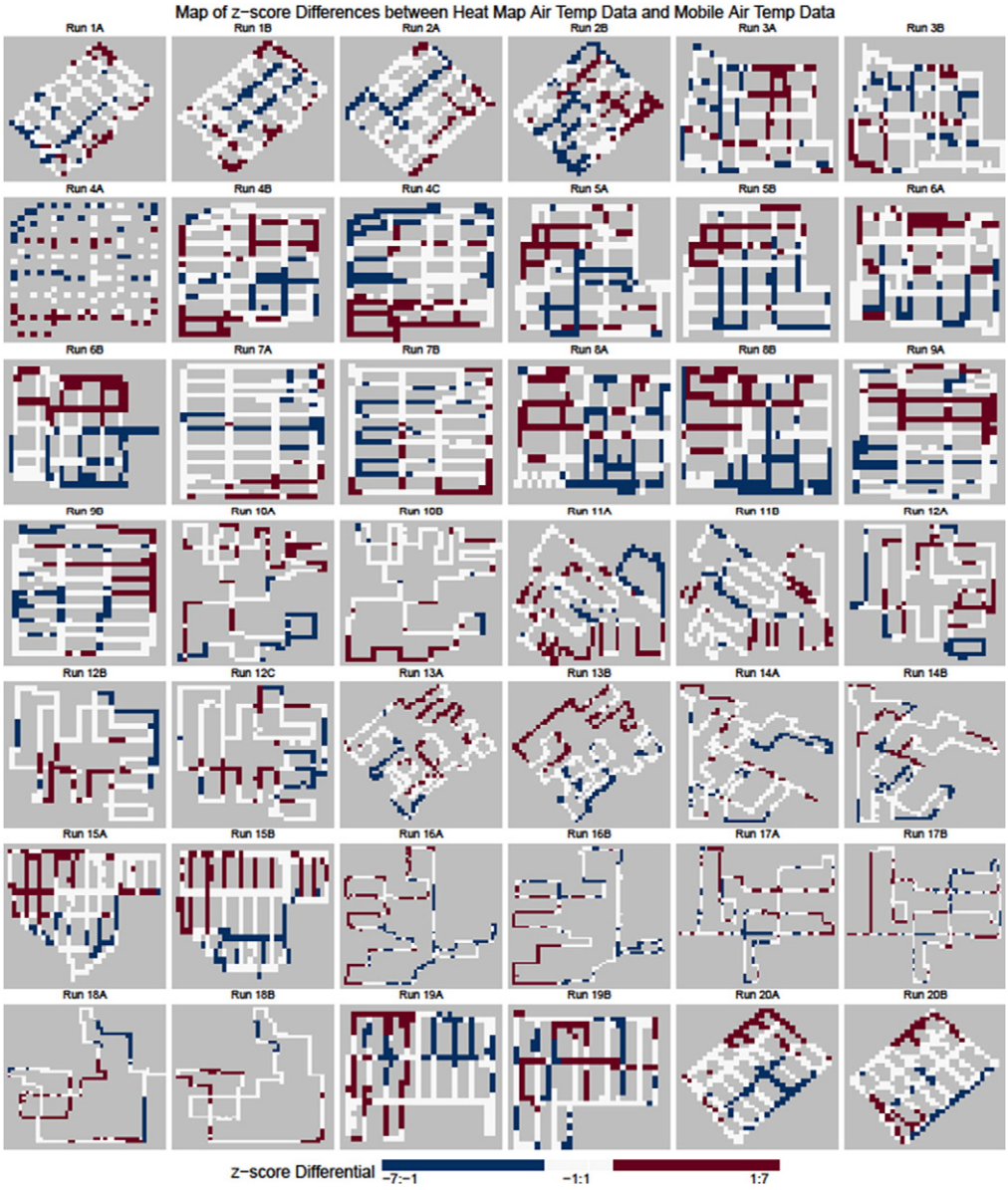

Fig. 5. Differences in the z-scores between the Greater Vancouver heat map (GVHM) and mobile air temperatures for all 42 runs. When interpreting, a positive z-score differential means that GVHM z-scores were higher than the mobile air temperature z-scores, suggesting that the GVHM overestimated air temperature. A negative differential suggests the GVHM underestimated air temperature.

LST was compared with daily maximum air temperature (Mostovoy et al., 2006). One possible explanation for our lower correlations was the 4–7 hour time gap between LST and mobile air temperature measurements, which would weaken any existing relationship. Another possible explanation is that we used mobile measurements from a single day while most previous studies used years of data from fixed weather stations or observations from sites throughout all seasons (Sohrabinia et al., 2014; Gallo et al., 2010). In addition, most of the other studies compared LST with time-matched or daily maximum air temperature at specific fixed pixels over time, which removes potential confounding by geographic variables such as land use/land cover

and temporal variation of thermal state. One study in Hong Kong did compare LST to 148 km of vehicular air temperature traverse data at a 10-meter resolution and found a r^2 of 0.80 (Nichol et al., 2009). However, when the results were split based on urban or rural classification of data, the r^2 value dropped to 0.42 for urban areas (Nichol et al., 2009).

Another possible factor in our lower r^2 values is the way that temperatures are measured by the different instruments. Air temperature sensors have an ellipsoid source area with both horizontal and vertical influences upwind of the sensor (Oke, 2004; Stewart and Oke, 2012; Schmid, 2002), while LST sensors have a circular source area below the sensor (Oke, 2004; Schmid, 1997). While this mismatch affects all measurements of the two variables, it may be exaggerated for microscale variables because of smaller overlapping areas. Another consideration is that all satellite-based LST measurements have some blurring between adjacent pixels, primarily due to the scanning process of the moving sensor. As such, these LST measurements may not truly represent variability at the microscale. Furthermore, Landsat 7 and 8 thermal data were natively recorded on 60 and 100 meter grids respectively, and are then resampled to a 30 meter grid, which results in blurring between neighbouring 30 meter pixels (USGS, 2016a). Calibration of LST measurements from Landsat 7 ETM + and its predecessor instruments have been ongoing for decades (Barsi et al., 2003), but spatial blurring is not relevant during these calibrations as they focus on homogeneous areas where absolute in-situ LST values can be measured. Without specific information on the influence of this blurring, we followed numerous other studies and compared in-situ measurements to the LST values from the pixels in which they were taken (Nichol and To, 2012; Sohrabinia et al., 2014; Benali et al., 2012; Nichol et al., 2009; Nichol and Wong, 2008; Mostovoy et al., 2006).

Heat maps generated by regression models provide useful estimates and visualizations of air temperature differences between areas. However, like any model estimates, they must be evaluated with real data to assess their validity, preferably at the same resolution as the maps themselves. Microscale mobile air temperature data fill a gap that other data sources cannot by offering accurate measurements collected at very high spatial resolutions with temporal coverage limited only by the study design and resources. Spatial coverage is limited by the distance a person can cover on foot, restricting the utility of this approach to smaller areas. However, it could have a wide range of applications such as heat map development, studying the land use/land cover drivers of microscale air temperature variability, or evaluation of more common and less resource-intensive methods.

Most heat maps are evaluated using cross-validation. Leave-one-out cross-validation for the GVHM involved (Zhang et al., 2014) leaving out all observations from one weather station, (Harlan et al., 2006) running the model, (Kalkstein and Davis, 1989) calculating the difference between the modelled temperature value and actual station temperature values, (Robine et al., 2008) repeating the procedure until the model has been run with each station missing once, and (Luber and McGeehin, 2008) calculating the average mean absolute error and root means square error for all runs to quantify accuracy (Ho et al., 2016a). One study in Hong Kong constructed 10-m resolution daytime and nighttime air temperature heat maps by regressing ASTER images with air temperature measurements collected within 1.5 h of the corresponding overpass (Nichol and To, 2012). These heat maps were validated with time-matched air temperature data from the Hong Kong fixed automatic weather station (AWS) network. The daytime heat map and AWS air temperature data had a correlation of 0.75, while the nighttime heat map and the AWS air temperature data had a correlation of 0.84 (Nichol and To, 2012). In comparison, we found a wide range of spatial correlation between patterns observed in the GVHM and measured in our data.

One limitation of our study is that land-sea and mountain-valley wind system shifts are common in greater Vancouver, which could generate within-run spatially-independent variability in the mobile data. However, an analysis of wind speed and direction patterns showed that the processes stayed fairly consistent during all mobile runs (not shown). Another limitation is the within-run correction for temporal trend, which assumes that the rate of change at fixed stations is comparable with the rate of change in mobile measurements. The correction was shown to be effective, however, as r^2 values between LST and the mobile air temperatures increased after the correction equation was applied to the mobile data (not shown). Another limitation is the between-day and time-of-day variability present in the mobile air temperature data, despite all sampling being conducted during summer months at approximately the same time of day. Time-of-day variability was minimized with the within-run air temperature correction, but we could not make credible corrections for between-day variability. The between-day variability was highlighted by the large differences between run replicates. This raises concern about the true average microscale air temperature at each route, and

necessitates treating all runs as unique samples. We suggest that future studies should prioritize route replicates over the number of routes monitored.

5. Conclusion

This study was conducted to assess the GVHM and two of its inputs with respect to their ability to reflect microscale variability in air temperature. Our results suggested that: (1) the limitations of fixed site air temperature measurements should be considered when assessing public health risk; (2) the correlations between microscale air temperature and LST may be highly variable; and (3) microscale data can be valuable for assessing heat maps developed with local and macroscale data. Future microscale mobile monitoring campaigns should focus on having more replicates for each route, keeping protocols consistent for each replicate, and monitoring fewer routes if limited by resources. Having many replicate measurements in fewer areas will provide a better representation of the true average of the spatial patterns.

Acknowledgements

We would like to acknowledge the Pacific Institute for Climate Solutions and the University of British Columbia for their support and funding of this research. We would also like to acknowledge Metro Vancouver for providing us with 1-minute frequency fixed weather station data. Finally, thanks to our insightful reviewers for helping to make this a stronger paper.

Appendix A. Supplementary material

Supplementary material associated with this article can be found in the online version, at doi: 10.1016/j.uclim.2016.10.001. These include various tables and figures which add background information to the overall study.

References

Barriopedro, D., Fischer, E.M., Luterbacher, J., Trigo, R.M., García-Herrera, R., 2011 Apr 8. The hot summer of 2010: redrawing the temperature record map of Europe. Science 332 (6026), 220–224.

Barsi, J.A., Barker, J.L., JR, S., 2003. An Atmospheric Correction Parameter Calculator for a single thermal band earth-sensing instrument. IEEE. 5:pp. 3014–3016 [cited 2015 Aug 11]. (Available from: http://ieeexplore.ieee.org/articleDetails.jsp?arnumber=1294665).

Benali, A., Carvalho, A.C., Nunes, J.P., Carvalhais, N., Santos, A., 2012 Sep. Estimating air surface temperature in Portugal using MODIS LST data. Remote Sens. Environ. 124, 108–121.

Cassano, J.J., 2013 Aug 9. Weather bike: a bicycle-based weather station for observing local temperature variations. Bull. Am. Meteorol. Soc. 95 (2), 205–209.

Eliasson, I., Svensson, M.K., 2003 Jun 1. Spatial air temperature variations and urban land use — a statistical approach. Meteorol. Appl. 10 (2), 135–149.

Emmanuel, R., Krüger, E., 2012 Jul. Urban heat island and its impact on climate change resilience in a shrinking city: the case of Glasgow, UK. Build. Environ. 53, 137–149.

Esri, 2014. ArcGIS 10.2. Environmental Science Research Institute, Redlands, CA .

Gallo, K., Hale, R., Tarpley, D., Yu, Y., 2010 Oct 4. Evaluation of the relationship between air and land surface temperature under clear- and cloudy-sky conditions. J. Appl. Meteorol. Climatol. 50 (3), 767–775.

García-Herrera, R., Díaz, J., Trigo, R.M., Luterbacher, J., Fischer, E.M., 2010 Mar 5. A review of the European summer heat wave of 2003. Crit. Rev. Environ. Sci. Technol. 40 (4), 267–306.

Gislason, P.O., Benediktsson, J.A., Sveinsson, J.R., 2006 Mar. Random forests for land cover classification. Pattern Recogn. Lett. 27 (4), 294–300.

Harlan, S.L., Brazel, A.J., Prashad, L., Stefanov, W.L., Larsen, L., 2006 Dec. Neighborhood microclimates and vulnerability to heat stress. Soc. Sci. Med. 63 (11), 2847–2863.

Hedquist, B.C., Brazel, A.J., 2006. Urban, residential, and rural climate comparisons from mobile transects and fixed stations: phoenix, Arizona. J. Ariz. Nev. Acad. Sci. 38 (2), 77–87.

Henderson, S.B., Kosatsky, T., 2012 Jun. A data-driven approach to setting trigger temperatures for heat health emergencies. Can. J. Public Health 103 (3), 227–230.

Ho, H.C., Knudby, A., Xu, Y., Hodul, M., Aminipouri, M., 2016 Feba. A comparison of urban heat islands mapped using skin temperature, air temperature, and apparent temperature (Humidex), for the greater Vancouver area. Sci. Total Environ. 544, 929–938.

Ho, H.C., Knudby, A., Walker, B.B., Henderson, S.B., 2016 Jun 27b. Delineation of spatial variability in the temperature-mortality relationship on extremely hot days in Greater Vancouver, Canada. Environ. Health Perspect. [Internet]. ([cited 2016 Jul 3]; Available from: http://ehp.niehs.nih.gov/EHP224).

Holmer, B., Thorsson, S., Eliasson, I., 2007 Jan 1. Cooling rates, sky view factors and the development of intra-urban air temperature differences. Geogr. Ann. Ser. Phys. Geogr. 89 (4), 237–248.

Intergovernmental Panel on Climate Change, 2014. Climate Change 2014: Impacts, Adaptation, and Vulnerability [Internet]. 1. IPCC [cited 2015 Apr 10]. Available from:. http://www.ipcc.ch/report/ar5/wg2/ .
Irons, J., Taylor, M., 2011. Landsat 7 Data Science Users Handbook [Internet]. ([cited 2015 Jul 10]. Available from: http://landsathandbook.gsfc.nasa.gov/).
Kaiser, R., Le Tertre, A., Schwartz, J., Gotway, C.A., Daley, W.R., Rubin, C.H., 2007 Apr. The effect of the 1995 heat wave in Chicago on all-cause and cause-specific mortality. Am. J. Public Health 97 (Suppl. 1), S158–S162.
Kalkstein, L., Davis, R., 1989 Mar 1. Weather and human mortality: an evaluation of demographic and interregional responses in the United States. Ann. Assoc. Am. Geogr. 79 (1), 44–64.
Kosatsky, T., Henderson, S.B., Pollock, S.L., 2012 Dec. Shifts in mortality during a hot weather event in Vancouver, British Columbia: rapid assessment with case-only analysis. Am. J. Public Health 102 (12), 2367–2371.
Luber, G., McGeehin, M., 2008 Nov. Climate change and extreme heat events. Am. J. Prev. Med. 35 (5), 429–435.
Lugo-Amador, N.M., Rothenhaus, T., Moyer, P., 2004 May. Heat-related illness. Emerg. Med. Clin. North Am. 22 (2), 315–327.
Markham, B., Barsi, J., 2014. Atmospheric Correction Parameter Calculator [Internet]. ([cited 2015 Aug 11]. Available from: http://atmcorr.gsfc.nasa.gov/).
Meehl, G.A., Tebaldi, C., 2004 Aug 13. More intense, more frequent, and longer lasting heat waves in the 21st century. Science 305 (5686), 994–997.
Met One Instruments, Inc. MODEL 064-1, 064-2, 2005. Temperature Sensor Operation Manual Document No 064-9800 .
Metro Vancouver, 2012. Station Information: Lower Fraser Valley Air Quality Monitoring Network .
Metro Vancouver, 2014. Metro Vancouver Weather Station Data: May-Sept 2014 .
Metro Vancouver, 2015. About Us [Internet]. ([cited 2015 Oct 25]. Available from: http://www.metrovancouver.org/about/Pages/default.aspx).
Mills, G., Foley, M., 2016. WUDAPT Vancouver local climate zone map [Internet]. World Urban Database and Access Portal Tools ([cited 2016 Sep 20]. Available from: http://www.wudapt.org/cities/in-the-americas/).
Mostovoy, G.V., King, R.L., Reddy, K.R., Kakani, V.G., Filippova, M.G., 2006 Mar 1. Statistical estimation of daily maximum and minimum air temperatures from MODIS LST data over the state of Mississippi. GIScience Remote Sens. 43 (1), 78–110.
NASA, 2014. About Landsat Science [Internet]. Landsat Science – About – Landsat Then and Now. ([cited 2014 Nov 6]. Available from: http://landsat.gsfc.nasa.gov/?page_id=2).
Nichol, J.E., To, P.H., 2012 Nov. Temporal characteristics of thermal satellite images for urban heat stress and heat island mapping. ISPRS J. Photogramm. Remote Sens. 74, 153–162.
Nichol, J.E., Wong, M.S., 2008 Dec 1. Spatial variability of air temperature and appropriate resolution for satellite-derived air temperature estimation. Int. J. Remote Sens. 29 (24), 7213–7223.
Nichol, J.E., Fung, W.Y., Lam, K., Wong, M.S., 2009 Oct. Urban heat island diagnosis using ASTER satellite images and "in situ" air temperature. Atmos. Res. 94 (2), 276–284.
Oke, T.R., 1982 Jan 1. The energetic basis of the urban heat island. Q. J. R. Meteorol. Soc. 108 (455), 1–24.
Oke, T.R., 1987. Boundary Layer Climates. Second edition. 435. Methuen Lond.
Oke, T.R., 2004. Initial Guidance to Obtain Representative Meteorological Observations at Urban Sites. 81. World Meteorological Organization Geneva.
Oke, T.R., Hay, J.E., 1994. The Climate of Vancouver. Second edition. BC Geographical SeriesUniversity of British Columbia, p. 91.
Oke, T.R., Maxwell, G.B., 1967. Urban heat island dynamics in Montreal and Vancouver. Atmos. Environ. 9 (2), 191–200 1975 Feb.
R Core Team, 2014. R: a Language and Environment for Statistical Computing [Internet]. R Foundation for Statistical Computing, Vienna, Austria (Available from: http://www.R-project.org).
Richards, K., 2005 Jan 1. Urban and rural dewfall, surface moisture, and associated canopy-level air temperature and humidity measurements for Vancouver, Canada. Bound.-Layer Meteorol. 114 (1), 143–163.
Rinner, C., Hussain, M., 2011 Jun 21. Toronto's urban Heat Island—exploring the relationship between land use and surface temperature. Remote Sens. 3 (6), 1251–1265.
Robine, J.-M., Cheung, S.L.K., Le Roy, S., Van Oyen, H., Griffiths, C., Michel, J.-P., et al., 2008 Feb. Death toll exceeded 70,000 in Europe during the summer of 2003. C. R. Biol. 331 (2), 171–178.
Saaroni, H., Ziv, B., 2010 Jun 7. Estimating the urban Heat Island contribution to urban and rural air temperature differences over complex terrain: application to an Arid City. J. Appl. Meteorol. Climatol. 49 (10), 2159–2166.
Sardon, J.P., 2007 Mar. The 2003 heat wave. Euro. Surveill. Bull. Eur. Sur. Mal. Transm. Eur. Commun. Dis. Bull. 12 (3), 226.
Sauder, L.P., 2010. School of Business Custom Demographic Maps [Internet]. ([cited 2014 May 19]. Available from: http://abacus.library.ubc.ca.ezproxy.library.ubc.ca/handle/10573/42375).
Schmid, H.P., 1997 Nov 15. Experimental design for flux measurements: matching scales of observations and fluxes. Agric. For. Meteorol. 87 (2), 179–200.
Schmid, H.P., 2002 Dec 2. Footprint modeling for vegetation atmosphere exchange studies: a review and perspective. Agric. For. Meteorol. 113 (1–4), 159–183.
Semenza, J.C., Rubin, C.H., Falter, K.H., Selanikio, J.D., Flanders, W.D., Howe, H.L., et al., 1996 Jul 11. Heat-related deaths during the July 1995 heat wave in Chicago. N. Engl. J. Med. 335 (2), 84–90.
Shaposhnikov, D., Revich, B., Bellander, T., Bedada, G.B., Bottai, M., Kharkova, T., et al., 2014 May. Mortality related to air pollution with the Moscow heat wave and wildfire of 2010. Epidemiol. Camb. Mass. 25 (3), 359–364.
Sohrabinia, M., Zawar-Reza, P., Rack, W., 2014 Mar 7. Spatio-temporal analysis of the relationship between LST from MODIS and air temperature in New Zealand. Theor. Appl. Climatol. 119 (3–4), 567–583.
Statistics Canada, 2008. Census Geography - Geographic Attribute File [Internet]. ([cited 2016 Mar 11]. Available from: https://www12.statcan.gc.ca/census-recensement/2011/geo/ref/att-eng.cfm).
Statistics Canada, 2012. Greater Vancouver, British Columbia (Code 5915) and British Columbia (Code 59) (Table) [Internet]. ([cited 2015 Nov 26]. Available from: http://www12.statcan.gc.ca/census-recensement/2011/dp-pd/prof/index.cfm?Lang=E).
Stewart, I.D., Oke, T.R., 2012 May 25. Local climate zones for urban temperature studies. Bull. Am. Meteorol. Soc. 93 (12), 1879–1900.
Straka, J.M., Rasmussen, E.N., Fredrickson, S.E., 1996 Oct 1. A mobile mesonet for finescale meteorological observations. J. Atmos. Ocean. Technol. 13 (5), 921–936.

U.S. Geological Survey, 2013. Using the USGS Landsat 8 Product [Internet]. ([cited 2014 Dec 30]. Available from: http://landsat.usgs.gov/Landsat8_Using_Product.php).
U.S. Geological Survey, 2015a. EarthExplorer [Internet]. ([cited 2015 Jul 10]. Available from: http://earthexplorer.usgs.gov/).
U.S. Geological Survey, 2015b. SLC-off Products: Background [Internet]. ([cited 2016 Jan 7]. Available from: http://landsat.usgs.gov/products_slcoffbackground.php).
USGS, 2012. Landsat Thematic Mapper (TM) [Internet]. ([cited 2014 Sep 3]. Available from: https://lta.cr.usgs.gov/TM).
USGS, 2016a. What Are the Band Designations for the Landsat Satellites? [Internet]. ([cited 2016 Sep 18]. Available from: http://landsat.usgs.gov/band_designations_landsat_satellites.php).
USGS, 2016b. Landsat 8 (L8) Data Users Handbook [Internet]. ([cited 2016 Jun 24]. Available from: http://landsat.usgs.gov/l8handbook_appendixa.php).
Van de Griend, A.A., Owe, M., 1993. On the relationship between thermal emissivity and the normalized difference vegetation index for natural surfaces. Int. J. Remote Sens. 14 (6), 1119–1131.
Watkins, R., Palmer, J., Kolokotroni, M., 2007 Jan 1. Increased temperature and intensification of the urban heat island: implications for human comfort and urban design. Built. Environ. 33 (1), 85–96 1978-.
World Meteorological Organization, 2008. Guide to Meterological Instruments and Methods of Observation. 7th edition. Secretariat of the World Meteorological Organization .
Zhang, K., Li, Y., Schwartz, J.D., O'Neill, M.S., 2014 Jul. What weather variables are important in predicting heat-related mortality? A new application of statistical learning methods. Environ Res. 132, 350–359.